Experimental Section

Synthesis of B-VS_2/CC

All the chemicals are of analytical grade and used as received. In brief, a piece of as-received carbon cloth (CC, 1 cm × 4 cm) was calcinated at 300 °C for 1 h and then ultrasonically treated in concentrated HCl for 1 h, followed by cleaning with ethanol and distilled water several times. Afterwards, 15 mg of $Na_3VO_4 \cdot 10H_2O$ and 12 mg of thioacetamide were dissolved in 40 mL of distilled water, to which 0.5 mg of $NH_4HB_4O_7 \cdot 3H_2O$ was added with the assistance of ultrasonication. Then, the mixed solution was poured into the Teflon-lined stainless steel autoclave followed by immersing the pretreated CC. The autoclave was sealed and maintained in an electric oven at the temperature of 180 °C for 24 h. After cooling to room temperature, the obtained sample was washed with deionized water/ethanol several times, followed by annealing in a tube furnace at 400 ^{o}C for 2 h under Ar atmosphere to obtain B-VS_2/CC. For comparison, the pristine VS_2/CC was prepared by the same procedure without addition of $NH_4HB_4O_7 \cdot 3H_2O$.

Electrochemical measurements

Electrochemical measurements were performed on a CHI-660E electrochemical workstation in a three-electrode configuration including working electrode (CC sample), reference electrode (Ag/AgCl), and counter electrode (graphite rod). All potentials were referenced to the reversible hydrogen electrode (RHE). The RHE calibration was experimentally conducted in the high-purity hydrogen saturated 0.5 M $LiClO_4$ electrolyte by cyclic voltammeters curves, with using graphite rod and Pt wire as counter and working electrodes, respectively (Fig. S9). The NRR tests were conducted in an H-type two-compartment electrochemical cell separated by a Nafion 211 membrane[1-3]. An absorber was set at the end of cell to avoid the loss of produced NH_3 by N_2 flow. The Nafion membrane was pretreated by boiling it in 5% H_2O_2 solution for 1 h, 0.5 M H_2SO_4 for 1 h and deionized water for 1 h in turn. During each electrolysis, ultra-high-purity N_2 gas (99.999%) was continuously purged into the cathodic chamber at a flow rate of 20 mL min^{-1}. After each NRR electrolysis, the solution in absorber was poured back into the cathodic compartment for the NH_3 detection. The produced NH_3 and possible N_2H_4 were quantitatively determined by the indophenol blue method[4], and approach of Watt and Chrisp[5], respectively.

Determination of NH_3

Typically, 4 mL of electrolyte was removed from the electrochemical reaction vessel. Then 50 μL of solution containing NaOH (0.75 M) and NaClO (ρ_{Cl} = ~4.5), 500 μL of solution containing 0.32 M NaOH, 0.4 M $C_7H_6O_3Na$, and 50 μL of $C_5FeN_6Na_2O$ solution (1 wt%) were respectively added into the electrolyte. After standing for 2 h, the UV-vis absorption spectrum was measured and the concentration-absorbance curves were calibrated by the standard NH_4Cl solution with a series of concentrations.

NH_3 yield was calculated by the following equation:

$$\mathrm{NH_3\ yield}\ (\mu\mathrm{g\ h^{-1}\ mg_{cat.}^{-1}}) = \frac{c_{\mathrm{NH_3}} \times V}{t \times m} \tag{1}$$

Faradaic efficiency was calculated by the following equation:

$$\text{Faradaic efficiency (\%)} = \frac{3 \times F \times c_{\mathrm{NH_3}} \times V}{17 \times Q} \times 100\% \tag{2}$$

where $c\mathrm{NH_3}$ (μg mL^{-1}) is the measured NH_3 concentration, V (mL) is the volume of the electrolyte, t (h) is the reduction time and m (mg) is the mass loading of the catalyst on CC. F (96500 C mol^{-1}) is the Faraday constant, Q (C) is the quantity of applied electricity.

Determination of N_2H_4

Typically, 5 mL of electrolyte was removed from the electrochemical reaction vessel. The 330 mL of color reagent containing 300 mL of ethyl alcohol, 5.99 g of $C_9H_{11}NO$ and 30 mL of HCl were prepared, and 5 mL of color reagent was added into the electrolyte. After stirring for 10 min, the UV-vis absorption spectrum was measured and the concentration-absorbance curves were calibrated by the standard N_2H_4 solution with a series of concentrations.

Characterizations

X-ray diffraction (XRD) pattern was recorded on a

Rigaku D/max 2400 diffractometer. Transmission electron microscopy (TEM), high-resolution transmission electron microscopy (HRTEM) and high-angle annular dark field (HAADF)-scanning transmission electron microscopy (STEM) were carried out on a Tecnai G^2 F20 microscope. X-ray photoelectron spectroscopy (XPS) analysis was conducted on a PHI 5702 spectrometer. Electron paramagnetic resonance (EPR) measurements were performed on a Bruker ESP-300 spectrometer. Dinitrogen temperature-programmed desorption (N_2-TPD) profiles were collected on a Chem-BET 3000 (Quantachrome) apparatus. ^1H nuclear magnetic resonance (NMR) measurements were performed on a 500 MHz Bruker superconducting-magnet NMR spectrometer. Prior to NMR measurements, all the feeding gases ($^{14}N_2$, $^{15}N_2$ and Ar) were respectively purified by an acid trap (0.05 M H_2SO_4) to eliminate the potential NO_x and NH_3 contaminants.

Calculation details

Spin-polarized plane-wave density functional theory (DFT) calculations were carried out using a Cambridge sequential total energy package (CASTEP) program [6]. Perdew−Burke−Ernzerh of (PBE) of generalized gradient approximation (GGA) was employed to describe the exchange-correlation potential with considering the van der Waals (vdW) interactions by a DFT-D method. To ensure the convergence for the total energy, we adopted a plane-wave cutoff energy of 400 eV with a Monkhorst-Pack grid (4 × 4 × 1) for k-point sampling. Besides, the convergence of energy and forces was set to be 2×10^{-5} eV/atom and 0.01 eV/Å, respectively. VS_2 (001) slab was modeled by a 4×4 supercell, and a vacuum region of 15 Å was used to separate the adjacent slabs.

The Gibbs free energy (ΔG, 298 K) of reaction steps is calculated by [7]:

$$\Delta G = \Delta E + \Delta ZPE - T\Delta S \tag{3}$$

where ΔE is the adsorption energy, ΔZPE is the zero point energy difference and $T\Delta S$ is the entropy difference between the gas phase and adsorbed state. The ZPE and $T\Delta S$ energies of gas molecules were obtained from the NIST database, and those of various NRR intermediates were calculated by the vibrational frequencies, all of which are given in Table S2.

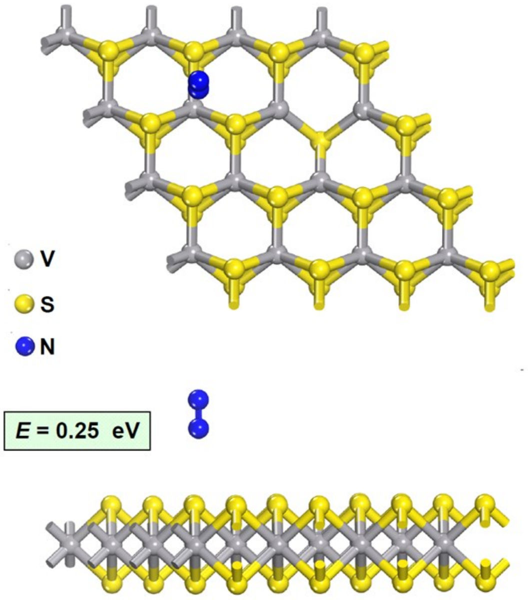

Fig. S1. Optimized structure of N_2 adsorption on pristine VS_2.

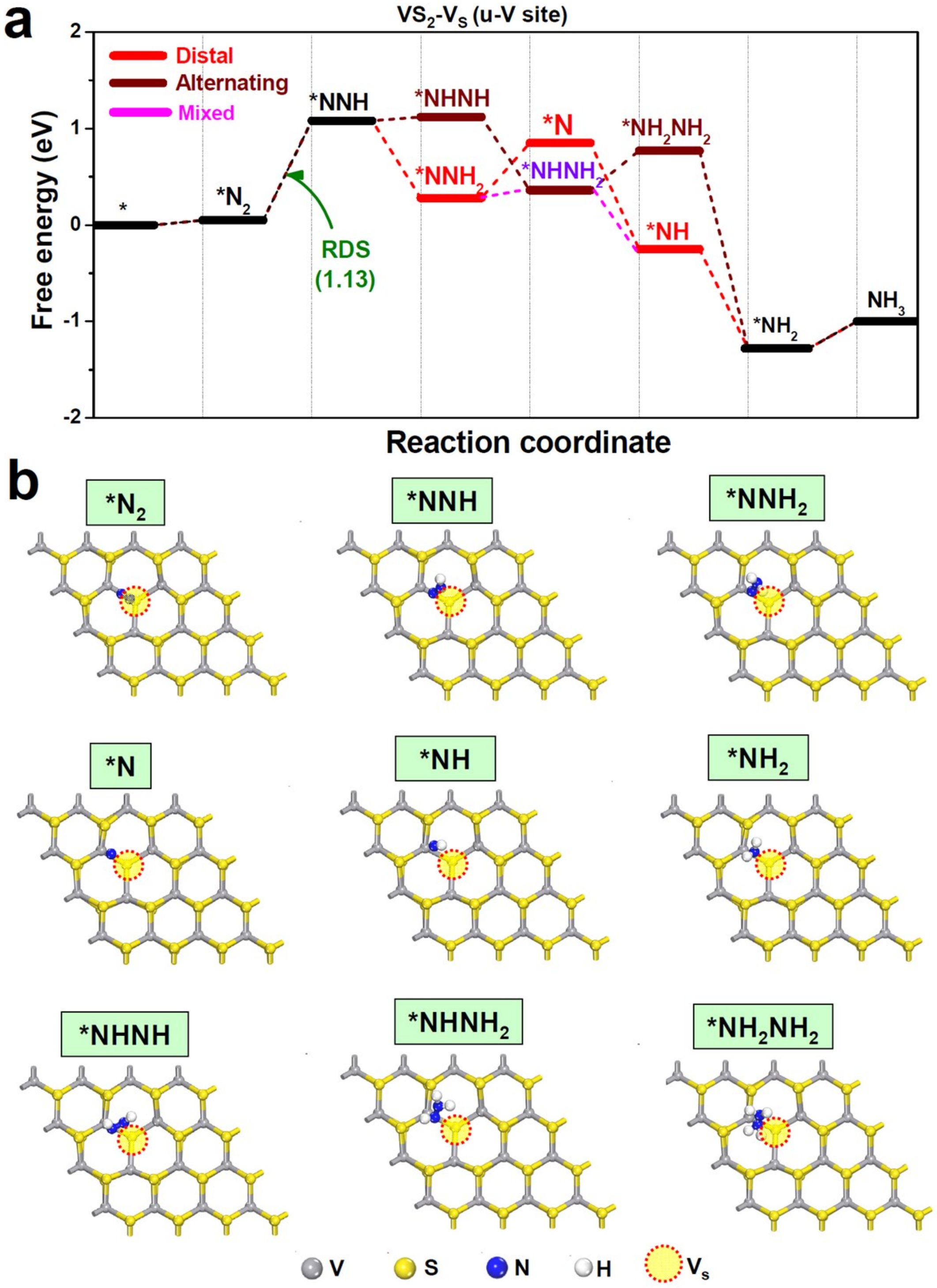

Fig. S2. (a) Free energy diagrams of distal, alternating and mixed NRR pathways on u-V site of VS_2-V_S at U = 0, and (b) corresponding optimized structures of NRR intermediates. It can be confirmed that **mixed pathway** is the most energetically preferred pathway.

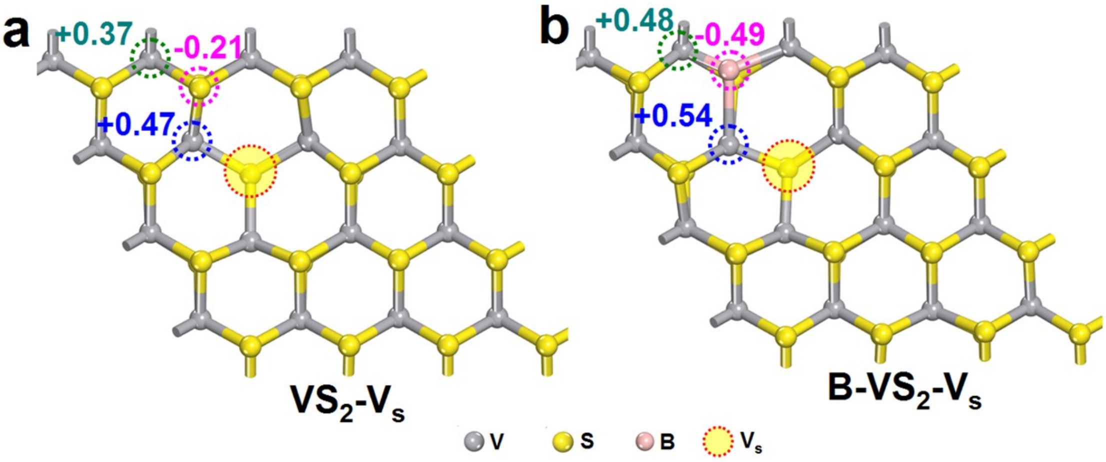

Fig. S3. Mulliken charge analysis of (a) VS_2-V_S and (b) B-VS_2-V_S.

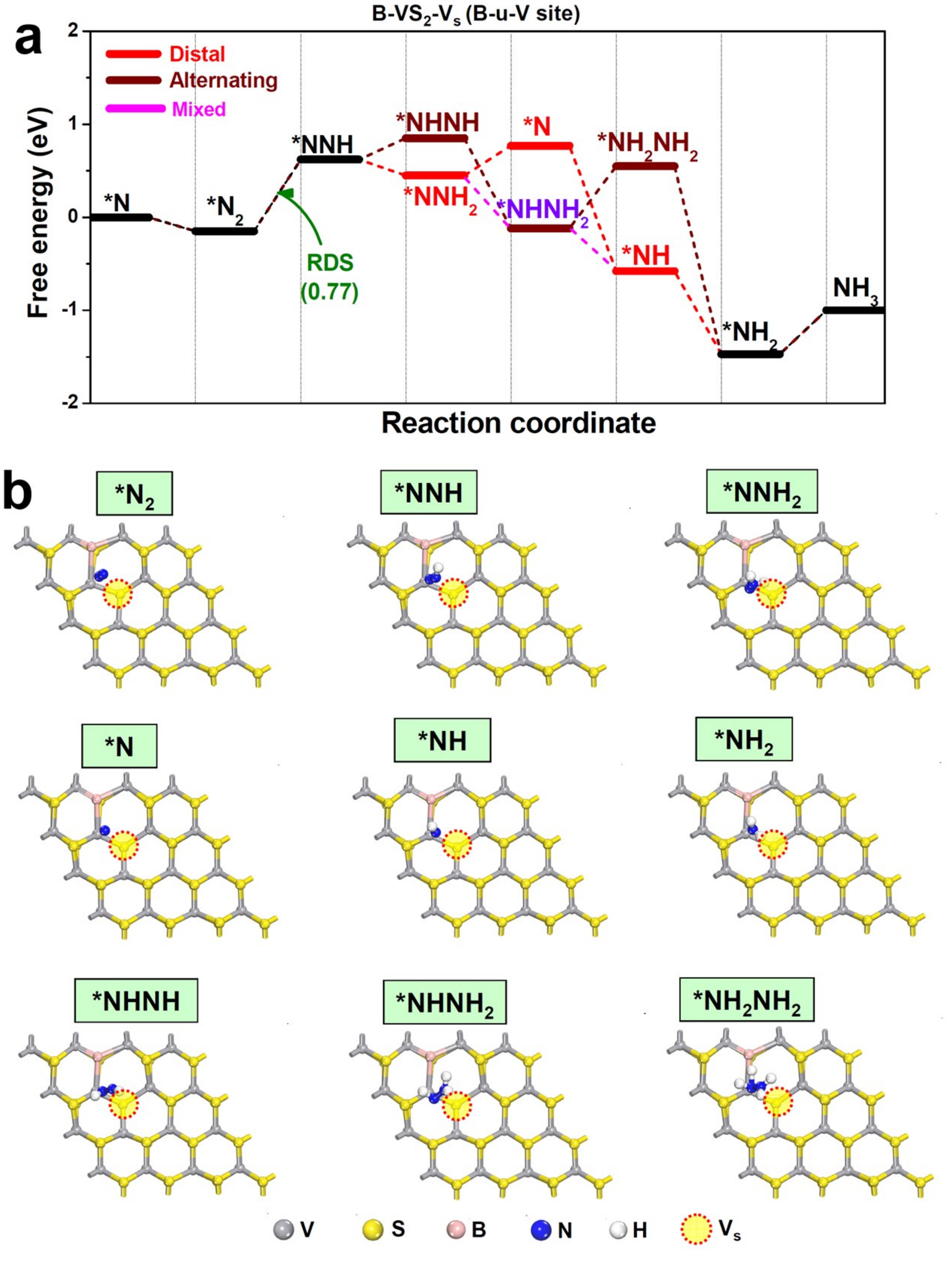

Fig. S4. Free energy diagrams of distal, alternating and mixed NRR pathways on B-u-V site of B-VS_2-V_S at U = 0, and (b) corresponding optimized structures of NRR intermediates. It can be confirmed that **mixed pathway** is the most energetically preferred pathway.

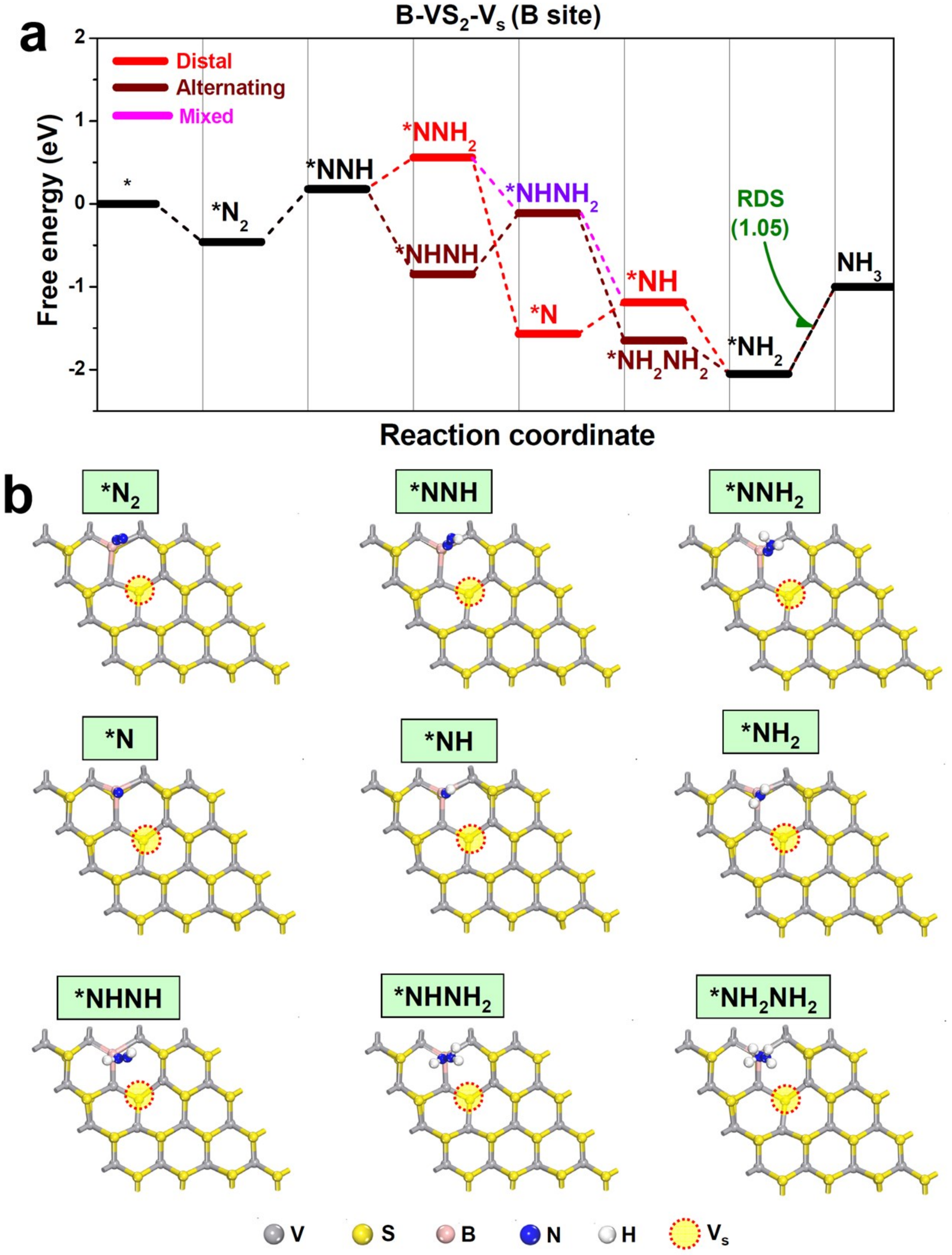

Fig. S5. Free energy diagrams of distal, alternating and mixed NRR pathways on B site of B-VS$_2$-V$_S$ at U = 0, and (b) corresponding optimized structures of NRR intermediates. It can be confirmed that the **distal pathway** is the most energetically preferred pathway.

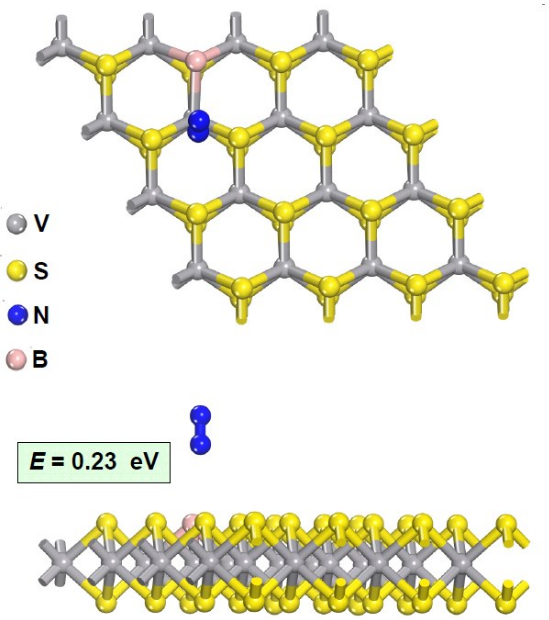

Fig. S6. Optimized structure of N_2 adsorption on B doped VS_2 without V_S.

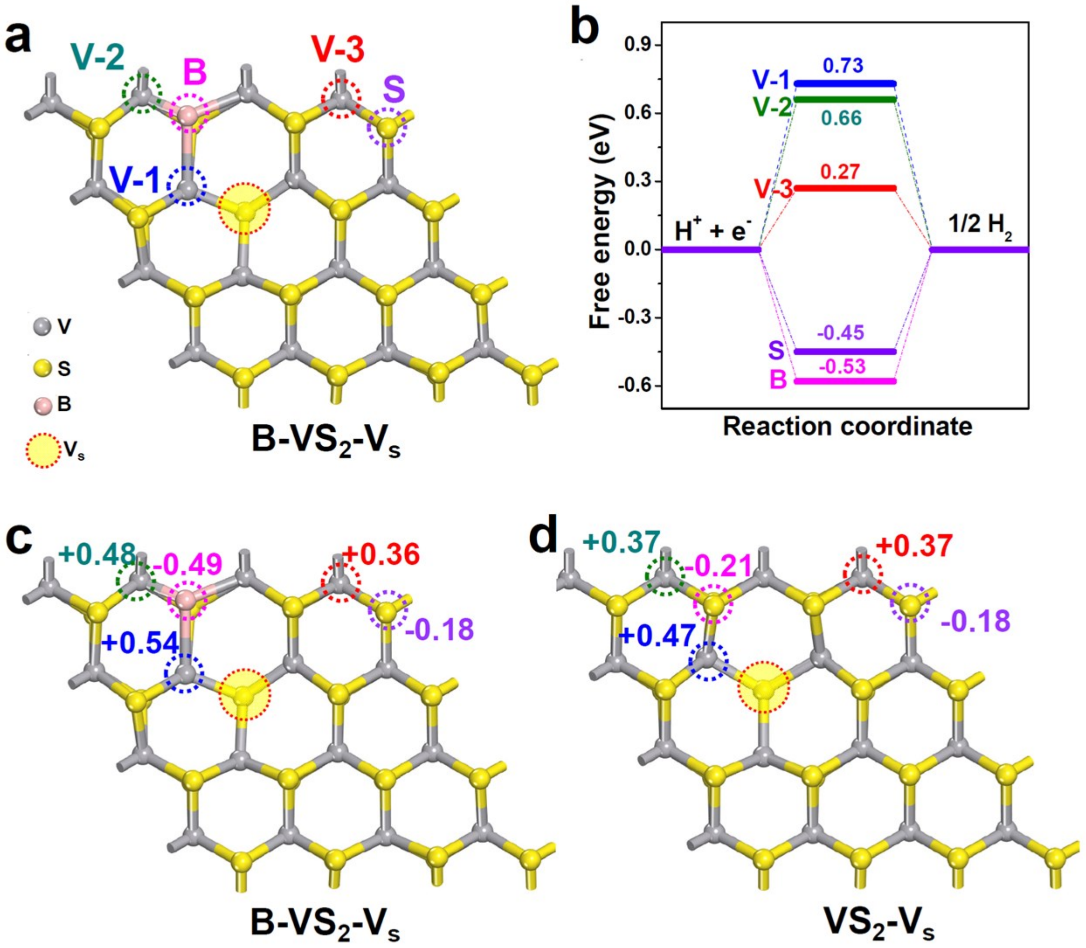

Fig. S7. (a) Marked sites of B-VS_2-Vs, and (b) their corresponding free energies of *H adsorption. (c, d) Mulliken charge analysis for the marked sites of (c) B-VS_2-V_S and (d) VS_2-V_S.

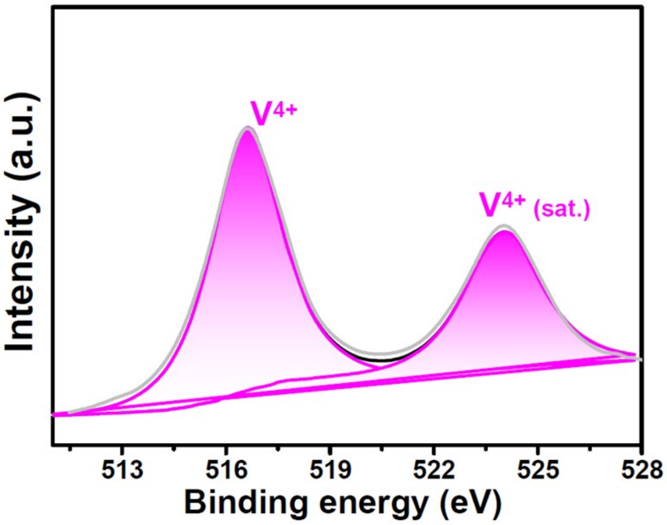

Fig. S8. XPS V2p spectra of commercial bulk VS_2.

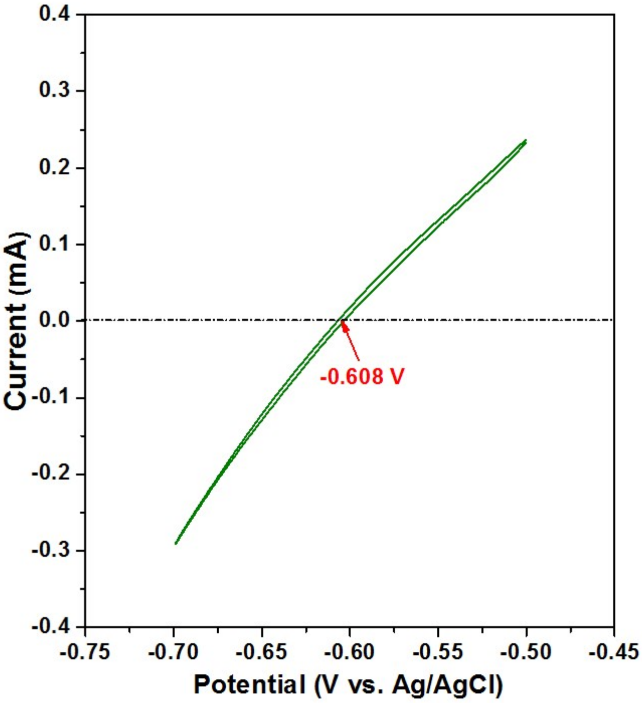

Fig. S9. The RHE calibration in 0.5 M $LiClO_4$ electrolyte.

The RHE calibration was conducted in the high-purity hydrogen saturated 0.5 M $LiClO_4$ electrolyte. The graphite rod and Pt wire were used as the counter and working electrodes, respectively. The cyclic voltammetry curves were performed at a scan rate of 1 mV s^{-1}. The RHE calibration potential for the hydrogen oxidation/evolution reactions is the average value of the two potentials at which the current crosses zero. It is shown in Fig. S9 that the *E*(RHE) is larger than *E*(Ag/AgCl) by 0.608 V. Therefore, we have *E*(RHE) = *E*(Ag/AgCl) +0.608.

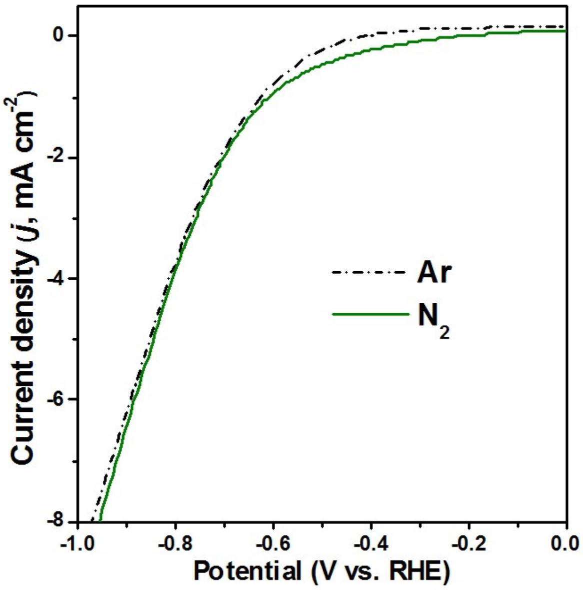

Fig. S10. LSV curves of B-VS_2/CC in Ar- and N_2- saturated solutions.

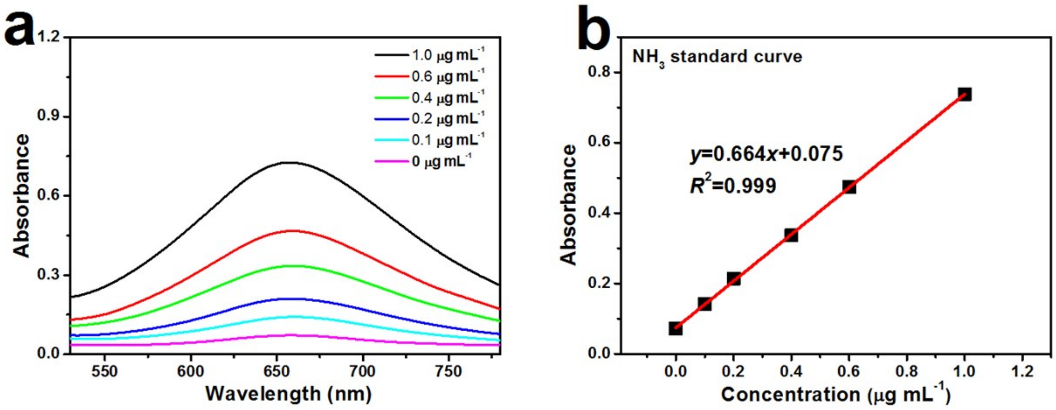

Fig. S11. (a) UV-Vis absorption spectra of indophenol assays with NH_4Cl after incubated for 2 h at ambient conditions. (b) Calibration curve used for calculation of NH_3 concentrations.

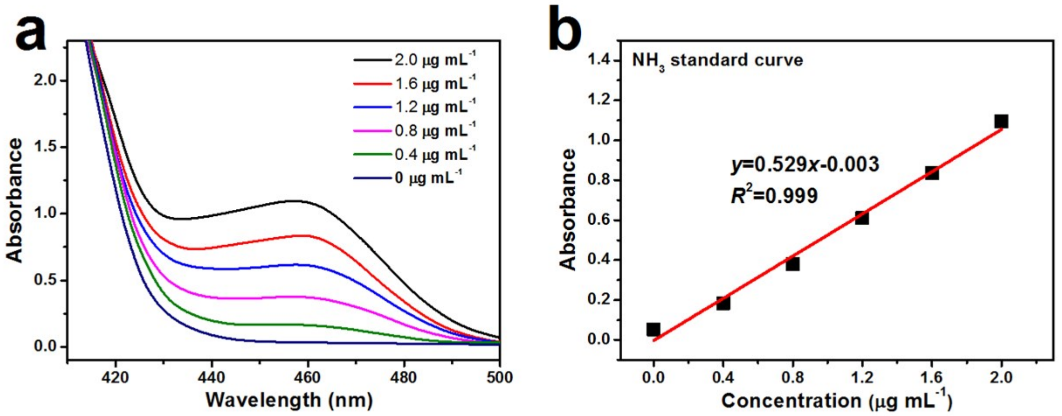

Fig. S12. (a) UV-Vis absorption spectra of N_2H_4 assays after incubated for 20 min at ambient conditions. (b) Calibration curve used for calculation of N_2H_4 concentrations.

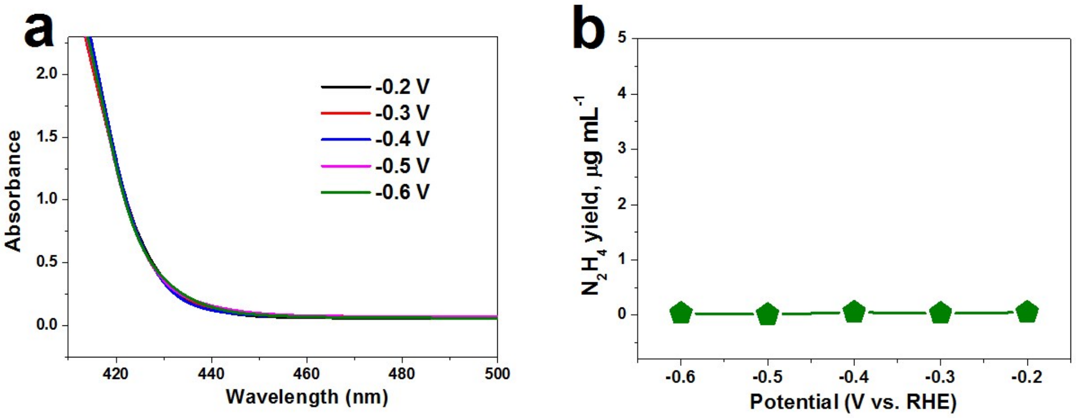

Fig. S13. (a) UV-Vis spectra of the electrolytes (stained with the chemical indicator based on the method of Watt and Chrisp) after 2 h electrocatalysis on B-VS_2/CC at various potentials, and (b) corresponding N_2H_4 concentrations in the electrolytes.

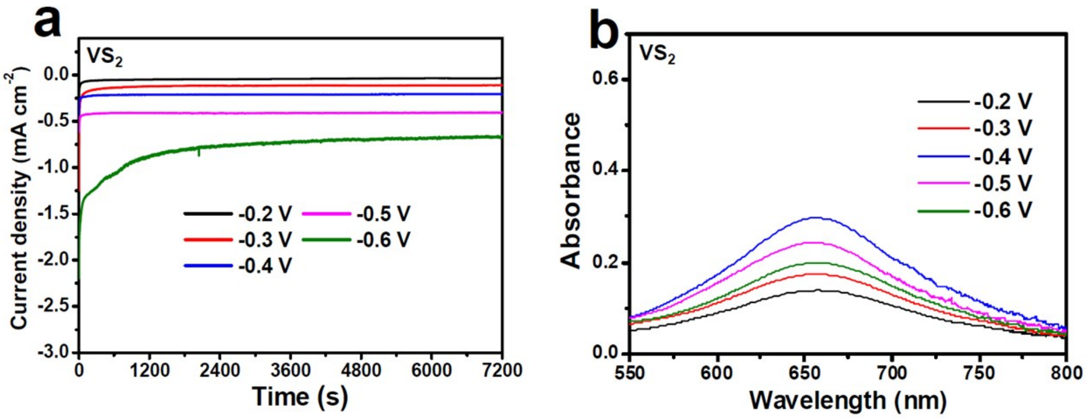

Fig. S14. Chronoamperometry test of B-VS$_2$/CC for 2 h of NRR electrolysis at various potentials, and (b) corresponding UV−vis absorption spectra of resultant electrolytes stained with indophenol indicator.

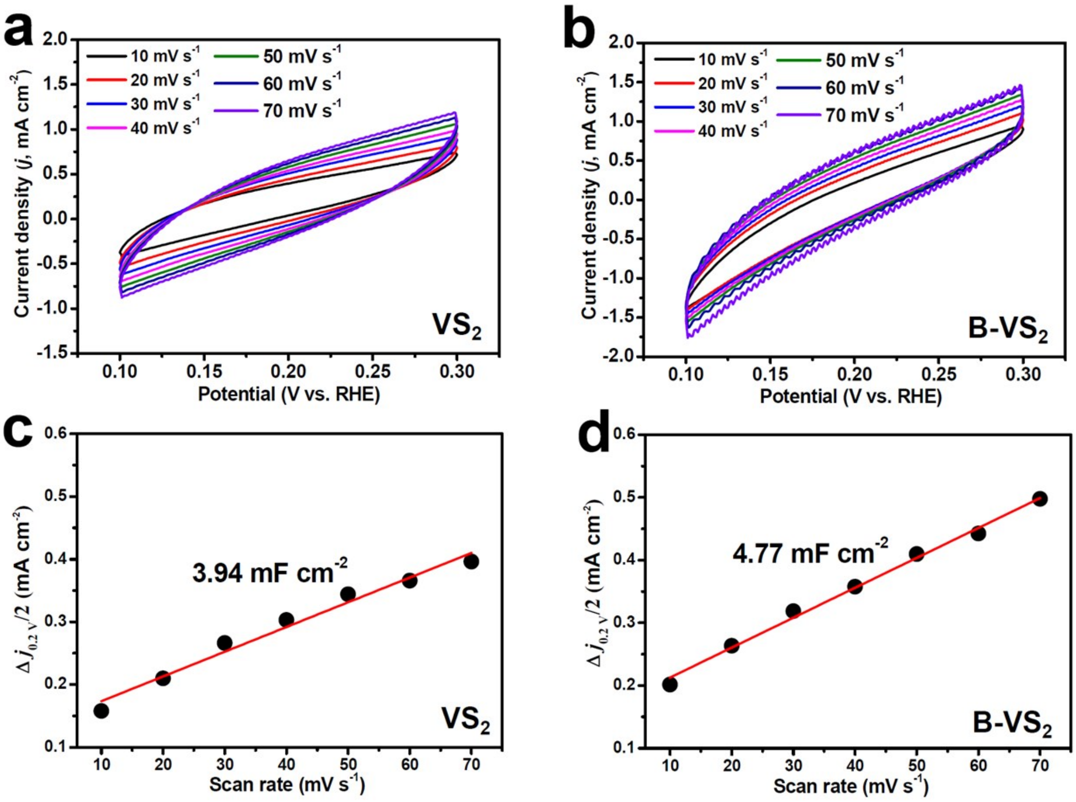

Fig. S15. Electrochemical double-layer capacitance (C_{dl}) measurements at different scanning rates of 10~70 mV s^{-1} for (a, c) VS_2/CC and (b, d) B-VS_2/CC.

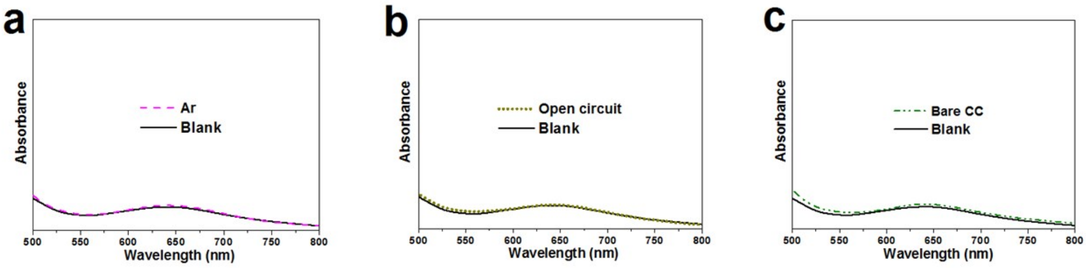

Fig. S16. UV-Vis absorption spectra of working electrolytes after 2 h of electrolysis in (a) Ar-saturated solutions on B-VS_2/CC at -0.4 V, (b) N_2-saturated solution on B-VS_2/CC at open circuit, and (c) N_2-saturated solution on pristine CC at -0.4 V. The blank data (without electrolysis) are also given for comparison.

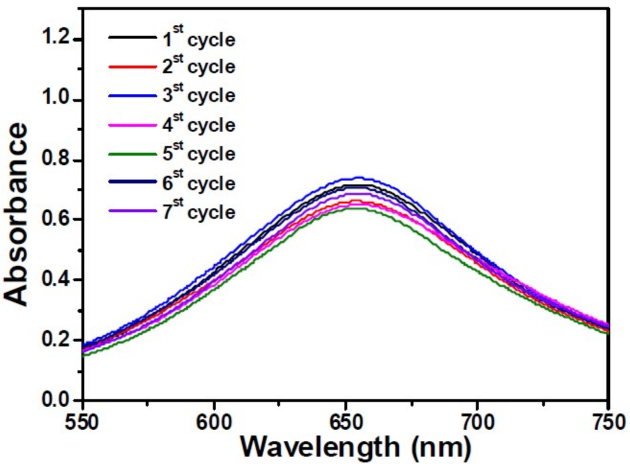

Fig. S17. UV-Vis absorption spectra of working electrolytes on B-VS_2/CC (each for 2 h electrolysis at -0.4 V) for seven cycles.

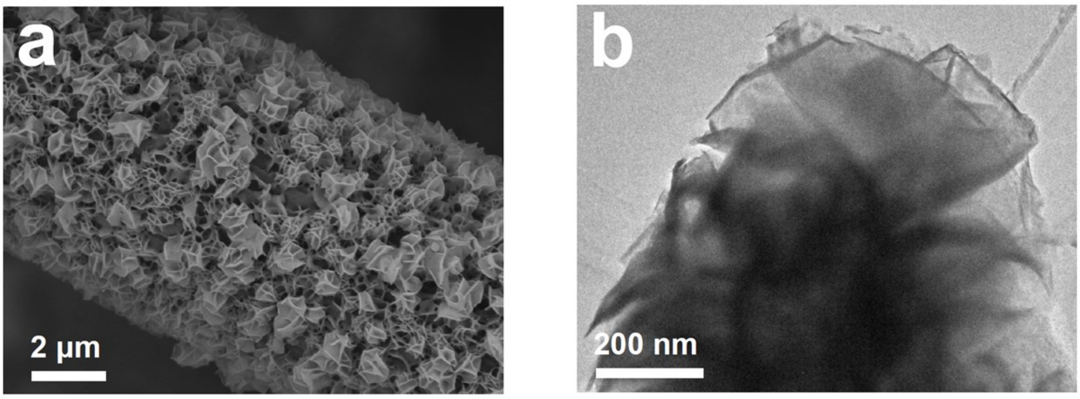

Fig. S18. Morphology of B-VS_2/CC after stability test. (a) SEM. (b) TEM.

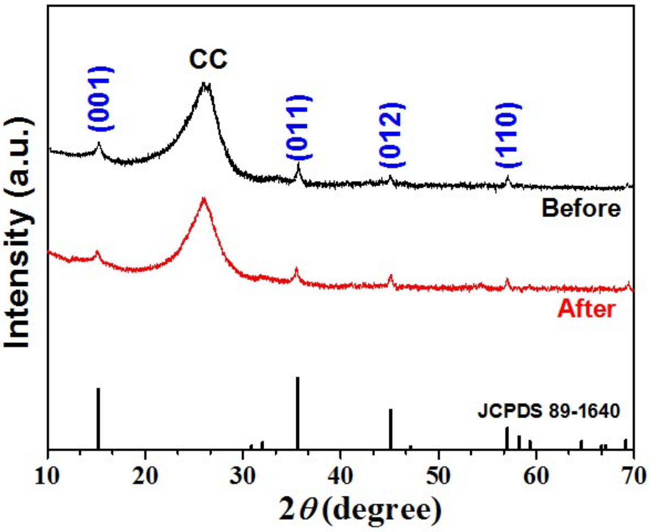

Fig. S19. XRD pattern of B-VS_2/CC before and after stability test.

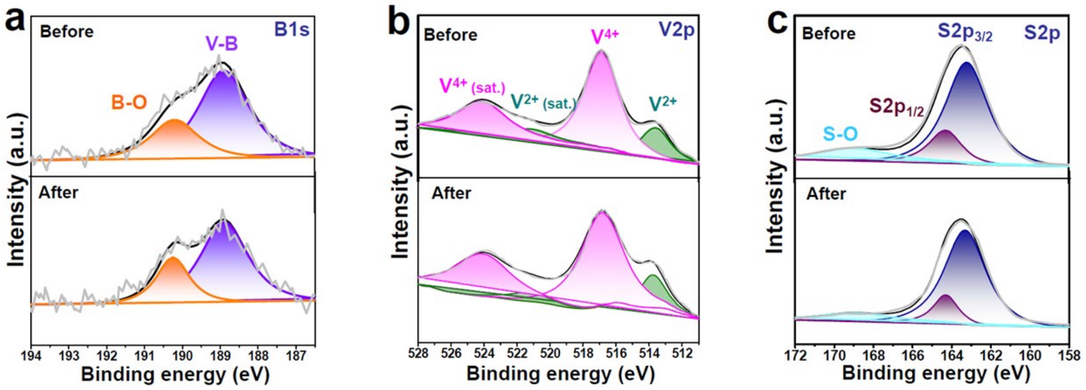

Fig. S20. XPS spectra of B-VS_2 nanosheets (scraped down from CC) before and after stability test: (a) B1s; (b) V2p; (c) S2p.

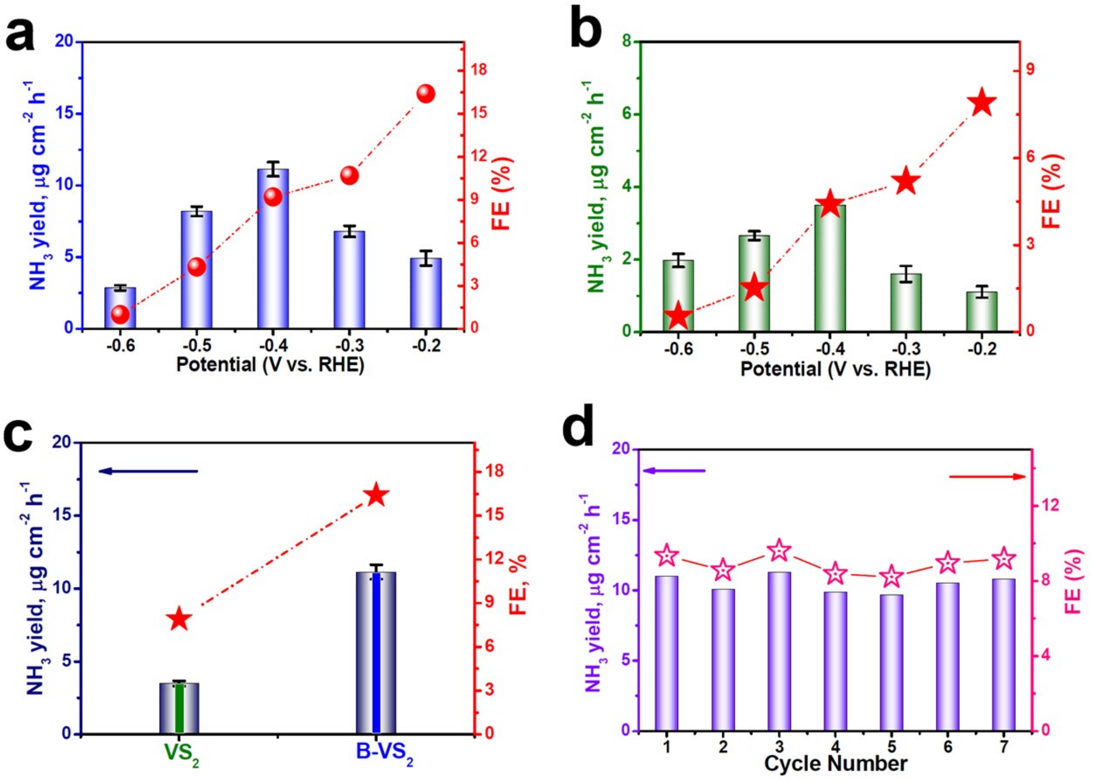

Fig. S21. All the figures related to NH_3 yield in the main text are provided with the unit of μg cm^{-2} h^{-1}. (a)-(d) correspond the Figs. 4c, d, e and Fig. 5c in the main text, respectively.

Table S1. Comparison of optimum NH_3 yield and Faradic efficiency (FE) for recently reported state-of-the-art NRR electrocatalysts at ambient conditions

Catalyst	Electrolyte	Determination method	Optimum Potential (V VS. RHE)	NH_3 yield	FE (%)	Ref.
B-doped graphene	0.05 M H_2SO_4	Indophenol blue method	-0.5	9.8 μg cm^{-2} h^{-1}	10.8	[8]
Mosaic Bi nanosheets	0.1 M Na_2SO_4	Indophenol blue method	-0.8	13.23 μg h^{-1} mg^{-1}	10.46	[9]
Black phosphorus	0.01 M HCl	Indophenol blue method	-0.7	31.37 μg h^{-1} mg^{-1}	5.07 (-0.6)	[10]
Sulfur-doped graphene	0.1 M HCl	Indophenol blue method	-0.6	27.3 μg h^{-1} mg^{-1}	11.5 (-0.5V)	[11]
Defective rich C_3N_4	0.1 M HCl	Indophenol blue method	-0.2	8.09 μg h^{-1} mg^{-1}	11.59	[12]
Fe_2O_3 nanorod	0.1 M Na_2SO_4	Indophenol blue method	-0.8	15.9 μg h^{-1} mg^{-1}	0.94	[13]
MoO_3 nanosheets	0.1 M HCl	Indophenol blue method	-0.5	29.43 μg h^{-1} mg^{-1}	1.9	[14]
MoO_2/graphene	0.1 M Na_2SO_4	Indophenol blue method	-0.35	37.4 μg h^{-1} mg^{-1}	6.6	[15]
MoS_2 with Li-S Interactions	0.1 M Li_2SO_4	Indophenol blue method	-0.2	43.4 μg h^{-1} mg^{-1}	9.81	[16]
Defect-rich MoS_2 nanoflower	0.1 M Na_2SO_4	Indophenol blue method	-0.4	29.28 μg h^{-1} mg^{-1}	8.34	[17]
Au/CeO_x-RGO	0.1 M KOH	Salicylate method	−0.2	8.31 μg h^{-1} mg^{-1}	10.1	[18]
Au@CeO_2	0.01 M H_2SO_4	Indophenol blue method	-0.4	28.2 μg h^{-1} mg^{-1}	9.5	[19]
Au-TiO_2 sub-nanocluster	0.1 M HCl	Indophenol blue method	-0.2	21.4 μg h^{-1} mg^{-1}.	8.11	[20]
Ru single atoms/NPC	0.05 M H_2SO_4	Indophenol blue method	-0.2	120.9 μg h^{-1} mg^{-1}	29.6	[21]
$Bi_4V_2O_{11}$-CeO_2 nanofibers	0.1 M HCl	Indophenol blue method	-0.2	23.21 μg h^{-1} mg^{-1}	10.16	[22]
Mo single atoms	0.1 M KOH	Indophenol blue method (NMR)	-0.3	34 μg h^{-1} mg^{-1}	14.6	[23]
Fe−N/C hybrid	0.1 M KOH	Indophenol blue method	-0.2	34.83 μg h^{-1} mg^{-1}	9.28	[24]
Mo_2C/C	0.5 M	Nessler's reagent	-0.3	11.3	7.8	[25]

	Li_2SO_4	method		μg h^{-1} mg^{-1}		
Sulfur dots-graphene nanohybrid	0.5 M $LiClO_4$	Indophenol blue method	-0.85	28.56 μg h^{-1} mg^{-1}	7.07	[26]
Hollow VO_2 microspheres	0.1 M Na_2SO_4	Indophenol blue method	-0.7	21.4 μg h^{-1} mg^{-1}	3.97	[27]
V_2O_3/C	0.1 M Na_2SO_4	Indophenol blue method	-0.6	12.3 μg h^{-1} mg^{-1}	7.28	[28]
VN nanoparticles	Nafion	Nessler's reagent method	-0.1	3.31×10^{-10} mol s^{-1} cm^{-2}	5.95	[29]
VN nanosheets	0.1 M HCl	Indophenol blue method	-0.5	8.40×10^{-11} mol s^{-1} cm^{-2}	2.25	[30]
VN nanowires	0.1 M HCl	Indophenol blue method	-0.3	2.48×10^{-10} mol s^{-1} cm^{-2}	3.58	[31]
B-VS_2/CC	**0.5 M $LiClO_4$**	**Indophenol blue method**	**-0.4**	**55.7** **μg h^{-1} mg^{-1}** **11.14** **μg cm^{-2} h^{-1}**	**16.4 (-0.2 V)**	**This work**

Table S2. Calculated ZPE and TΔS energies of various NRR intermediates

	△ZPE (eV)	**TΔS (eV)**
$*N_2$	0.23	0.11
*NNH	0.49	0.13
$*NNH_2$	0.85	0.15
*NHNH	0.88	0.12
$*NHNH_2$	1.18	0.11
$*NH_2NH_2$	1.55	0.12
*N	0.09	0.05
*NH	0.41	0.05
$*NH_2$	0.76	0.05
N_2	0.15	0.6
H_2	0.27	0.41
NH_3	0.89	0.74

Supplementary references

[1]. K. Chu, J. Wang, Y. P. Liu, Q. Q. Li and Y. L. Guo, *J. Mater. Chem. A*, 2020, **8**, 7117-7124.

[2]. K. Chu, Y. Liu, Y. Chen and Q. Li, *J. Mater. Chem. A*, 2020, **8**, 5200-5208.

[3]. K. Chu, Q. Li, Y. Liu, J. Wang and Y. Cheng, *Appl. Catal. B*, 2020, **267**, 118693.

[4]. D. Zhu, L. Zhang, R. E. Ruther and R. J. Hamers, *Nat. Mater.*, 2013, **12**, 836.

[5]. G. W. Watt and J. D. Chrisp, *Anal. Chem.*, 1952, **24**, 2006-2008.

[6]. S. J. Clark, M. D. Segall, C. J. Pickard, P. J. Hasnip, M. I. J. Probert, K. Refson and M. C. Payne, *Z. Kristallogr.*, 2005, **220**, 567-570.

[7]. A. A. Peterson, *Energy Environ. Sci.*, 2010, **3**, 1311-1315.

[8]. X. Yu, P. Han, Z. Wei, L. Huang, Z. Gu, S. Peng, J. Ma and G. Zheng, *Joule*, 2018, **2**, 1610-1622.

[9]. L. Li, C. Tang, B. Xia, H. Jin, Y. Zheng and S.-Z. Qiao, *ACS Catal.*, 2019, **9**, 2902-2908.

[10]. L. L. Zhang, L. X. Ding, G. F. Chen, X. F. Yang and H. H. Wang, *Angew. Chem. Int. Edit.*, 2019, **131**, 2638-2642.

[11]. L. Xia, J. Yang, H. Wang, R. Zhao, H. Chen, W. Fang, A. M. Asiri, F. Xie, G. Cui and X. Sun, *Chem. Commun.*, 2019, **55**, 3371-3374.

[12]. C. Lv, Y. Qian, C. Yan, Y. Ding, Y. Liu, G. Chen and G. Yu, *Angew. Chem. Int. Edit.*, 2018, **57**, 10246-10250.

[13]. X. Xiang, Z. Wang, X. Shi, M. Fan and X. Sun, *ChemCatChem*, 2018, **10**, 4530-4535.

[14]. J. Han, X. Ji, X. Ren, G. Cui, L. Li, F. Xie, H. Wang, B. Li and X. Sun, *J. Mater. Chem. A*, 2018, **6**, 12974-12977.

[15]. J. Wang, Y. P. Liu, H. Zhang, D. J. Huang and K. Chu, *Catal. Sci. Technol.*, 2019, **9**, 4248-4254.

[16]. Y. Liu, M. Han, Q. Xiong, S. Zhang, C. Zhao, W. Gong, G. Wang, H. Zhang and H. Zhao, *Adv. Energy. Mater.*, 2019, **9**, 1803935.

[17]. X. Li, T. Li, Y. Ma, Q. Wei, W. Qiu, H. Guo, X. Shi, P. Zhang, A. M. Asiri and L. Chen, *Adv. Energy. Mater.*, 2018, **8**, 1801357.

[18]. S. J. Li, D. Bao, M. M. Shi, B. R. Wulan, J. M. Yan and Q. Jiang, *Adv. Mater.*, 2017, **29**, 1700001.

[19]. G. Liu, Z. Cui, M. Han, S. Zhang, C. Zhao, C. Chen, G. Wang and H. Zhang, *Chem. Eur. J.*, 2019, **25**, 5904-5911.

[20]. M. M. Shi, D. Bao, B. R. Wulan, Y. H. Li, Y. F. Zhang, J. M. Yan and Q. Jiang, *Adv. Mater.*, 2017, **29**, 1606550.

[21]. Z. Geng, Y. Liu, X. Kong, P. Li, K. Li, Z. Liu, J. Du, M. Shu, R. Si and J. Zeng, *Adv. Mater.*, 2018, **30**, 1803498.

[22]. C. Lv, C. Yan, G. Chen, Y. Ding, J. Sun, Y. Zhou and G. Yu, *Angew. Chem. Int. Edit.*, 2018, **130**, 6181-6184.

[23]. L. Han, X. Liu, J. Chen, R. Lin, H. Liu, F. Lu, S. Bak, Z. Liang, S. Zhao and E. Stavitski, *Angew. Chem. Int. Edit.*, 2018, **58**, 2321-2325.

[24]. Y. Wang, X. Cui, J. Zhao, G. Jia, L. Gu, Q. Zhang, L. Meng, Z. Shi, L. Zheng and C. Wang, *ACS Catal.*, 2018, **9**, 336-344.

[25]. H. Cheng, L. X. Ding, G. F. Chen, L. Zhang, J. Xue and H. Wang, *Adv. Mater.*, 2018, **30**, 1803694.

[26]. H. Chen, X. Zhu, H. Huang, H. Wang, T. Wang, R. Zhao, H. Zheng, A. M. Asiri, Y. Luo and

X. Sun, *Chem. Commun.*, 2019, **55**, 3152-3155.

[27]. Q. Liu, R. Zhang, H. Guo, L. Yang, Y. Wang, Z. Niu, H. Huang, H. Chen, L. Xia and T. Li, *ChemElectroChem*, 2019, **6**, 1014-1018.

[28]. R. Zhang, J. Han, B. Zheng, X. Shi, A. M. Asiri and X. Sun, *Inorg. Chem. Front.*, 2019, **6**, 391-395.

[29]. X. Yang, J. Nash, J. Anibal, M. Dunwell, S. Kattel, E. Stavitski, K. Attenkofer, J. G. Chen, Y. Yan and B. Xu, *J. Am. Chem. Soc.*, 2018, **140**, 13387-13391.

[30]. R. Zhang, Y. Zhang, X. Ren, G. Cui, A. M. Asiri, B. Zheng and X. Sun, *ACS Sustain. Chem. Eng.*, 2018, **6**, 9545-9549.

[31]. X. Zhang, R.-M. Kong, H. Du, L. Xia and F. Qu, *Chem. Commun.*, 2018, **54**, 5323-5325.